Proceedings of the 17th World Congress
The International Federation of Automatic Control
Seoul, Korea, July 6-11, 2008

Reconfigurable Control of Hammerstein Systems after Actuator Faults

Jan H. Richter * **Jan Lunze** *

* *Institute of Automation and Computer Control (ATP), Ruhr-Universität Bochum, Universitätsstrasse 150, 44801 Bochum, Germany*
E-mail: {Richter|Lunze}@atp.rub.de.

Abstract: A new method for the control reconfiguration of stable Hammerstein systems after actuator faults is described. The class of Hammerstein systems contains input-saturated systems, which are ubiquitous in practice. The new reconfiguration approach uses a virtual actuator that permits to keep the nominal controller in the loop. The concept of virtual actuators is extended to reflect the nonlinear plant characteristics. A systematic procedure for virtual actuator design is presented that guarantees closed-loop stability. The approach is experimentally verified using a system of coupled tanks.

1. INTRODUCTION

Control reconfiguration is an approach to create dependable systems by means of appropriate feedback control (Rauch, 1995). It responds to severe component failures that break the control loop by restructuring the control loop on-line (Blanke et al., 2006). Control reconfiguration is an active fault-tolerant control methodology that uses the estimate $\hat{f}$ of the fault f, which is obtained from a diagnosis component (FDI) (Fig. 1). Valve blocking, rudder blockage and sensor outages are types of component failures covered by this paper. Furthermore, it is assumed here that the fault isolation task is solved and that the fault model is known.

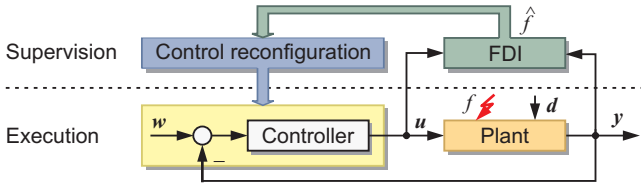

Fig. 1. Active fault-tolerant control scheme.

This paper presents a new automatic control reconfiguration method after actuator faults or failures for Hammerstein systems. The motivation for studying this class of systems arises from the observation that all practical systems are subject to input range limitations, which give rise to Hammerstein systems. In a prior case study of the authors, those input limitations were found to be a particularly limiting factor to the achievable reconfiguration performance (Richter et al., 2007).

Prior approaches to control reconfiguration of linear systems mostly replace the nominal controller with a new controller that is tailored to the faulty plant (Ashari et al., 2005; Staroswiecki et al., 2006; Chen and Saif, 2007). Little work on the control reconfiguration of nonlinear systems has been published (Bonivento et al., 2004; Jiang et al., 2006; Rodrigues et al., 2006). The mentioned approaches discard the nominal controller from the loop, which is undesirable for two reasons. First, the nominal controller is usually the result of repeated synthesis, testing and tuning steps rather than obtained in a single synthesis step. Secondly, if the controller is a human being, the replacement of the controller for reconfiguration implies the need for strong training efforts.

By contrast, in the present approach the nominal controller remains an integral part of the reconfigured closed loop. To this end, the concept of the virtual actuator is extended towards Hammerstein systems. The virtual actuator is a linear dynamical system that redirects the control inputs given by the nominal controller from lost or degraded actuators towards remaining control inputs (Steffen, 2005). The novelty of this paper consists in extending this concept to linear plants with static input-nonlinearities.

The paper proceeds as follows. The notation is introduced in Section 2. The Hammerstein virtual actuator is presented in Section 3, where the main result regarding closed-loop stability is stated. This result is proven in Section 4. The new design approach is summarised in Section 5. Experimental results using the new approach are shown in Section 6, and the paper concludes with Section 7.

2. MODELLING FRAMEWORK AND NOTATION

Linear disturbed Hammerstein systems are considered that consist of a strictly proper linear system, and a static input nonlinearity $\boldsymbol{f}: \mathbb{R}^m \to \mathbb{R}^m$,

$$\dot{\boldsymbol{x}}(t) = \boldsymbol{A}\boldsymbol{x}(t) + \boldsymbol{B}\boldsymbol{f}(\boldsymbol{u}_c(t)) + \boldsymbol{B}_d\boldsymbol{d}(t), \quad \boldsymbol{x}(0) = \boldsymbol{x}_0 \tag{1a}$$

$$\boldsymbol{y}(t) = \boldsymbol{C}\boldsymbol{x}(t), \tag{1b}$$

where $\boldsymbol{u}_c(t) \in \mathbb{R}^m$ is the control input, $\boldsymbol{x}(t) \in \mathbb{R}^n$ the state, $\boldsymbol{y}(t) \in \mathbb{R}^r$ the output, $\boldsymbol{d}(t) \in \mathbb{R}^q$ the disturbance, $\boldsymbol{A} \in \mathbb{R}^{n\times n}$ the state transition matrix, $\boldsymbol{B} \in \mathbb{R}^{n\times m}$ the input matrix, $\boldsymbol{B}_d \in \mathbb{R}^{n\times q}$ the disturbance matrix, and $\boldsymbol{C} \in \mathbb{R}^{r\times n}$ the output matrix.

Assumption 1. The nonlinear map $\boldsymbol{f}$ is assumed to be locally Lipschitz, radially bounded,

$$\exists \varepsilon > 0 \text{ s.t. } \forall \boldsymbol{u}_c(t): \ \|\boldsymbol{f}(\boldsymbol{u}_c(t))\| < \varepsilon, \tag{2}$$

and bounded in the sector $[\boldsymbol{K}_1, \boldsymbol{K}_2]$ with the lower bounds $\boldsymbol{K}_1$ and upper bounds $\boldsymbol{K}_2$.

The assumption on boundedness is not restrictive in practice, since the inputs to most physical plants are limited by energetic or kinematic constraints. Typically, $\boldsymbol{f}$ contains pairwise disjoint saturations

$$\forall i: \ \mathrm{sat}(\underline{u}_i, \overline{u}_i, u_i(t)) = \begin{cases} \underline{u}_i & \text{if } u_i(t) < \underline{u}_i \\ u_i(t) & \text{if } \underline{u}_i \le u_i(t) \le \overline{u}_i \\ \overline{u}_i & \text{else} \end{cases} \tag{3}$$

that individually saturate the input channels with the lower and upper bounds $\underline{\boldsymbol{u}}$ and $\overline{\boldsymbol{u}}$. The sector bounds $\boldsymbol{K}_1, \boldsymbol{K}_2$ of the function $\boldsymbol{f}$ are expressed in a matrix $\boldsymbol{D}$ not to be confused with the throughput matrix (Khalil, 2002). If the ith output of $\boldsymbol{f}$ only depends on the ith input, then $\boldsymbol{D} = \mathrm{diag}(1/D_i)$ is a diagonal matrix where each diagonal entry expresses the sector bound of that input channel,

$$1/D_i = \max_{u_i \in \mathbb{R}} f_i(u_i)/u_i, \quad i = 1, \ldots, m. \tag{4}$$

The control commands from the nominal controller $\boldsymbol{K}$,

$$\boldsymbol{u}_c(t) = \boldsymbol{K}(\boldsymbol{y}(t), \boldsymbol{w}(t)), \tag{5}$$

are denoted by $\boldsymbol{u}_c(t)$, where $\boldsymbol{w}(t)$ is the reference signal.

Assumption 2. The nominal closed loop (1), (5) is assumed to be globally asymptotically stable.

A function $\gamma : \mathbb{R}_{0+} \to \mathbb{R}_{0+}$ is of *class* $\mathcal{N}$ if it is continuous and nondecreasing. It is of *class* $\mathcal{N}_0$ if in addition it satisfies $\gamma(0) = 0$. A *class* $\mathcal{K}$ *function* is a function $\alpha \in \mathcal{K} : \mathbb{R}_{0+} \to \mathbb{R}_{0+}$ which is continuous, positive definite ($\geq$), strictly increasing, and satisfies $\alpha(0) = 0$. A *class* $\mathcal{K}_\infty$ *function* is a function $\alpha \in \mathcal{K}_\infty$ that is additionally unbounded. A *class* $\mathcal{KL}$ *function* is a function $\beta \in \mathcal{KL} : \mathbb{R}_{0+} \times \mathbb{R}_{0+} \to \mathbb{R}_{0+}$ such that $\beta(\cdot, t) \in \mathcal{K}_\infty$ for any fixed t, and for each fixed $r \geq 0, \beta(r, t) \to 0$ as $t \to \infty$.

Definition 1. (Input-to-state-stability (Sontag, 1989)). The system (1) is called *input-to-state-stable*, if $\exists \beta \in \mathcal{KL}, \gamma \in \mathcal{K}_\infty$ s. t. $|\boldsymbol{x}(t)| \leq \beta(|\boldsymbol{x}_0|, t) + \gamma(\|\boldsymbol{u}(t)\|_\infty)$ holds for all inputs $\boldsymbol{u}(t)$, all initial states $\boldsymbol{x}_0$, and all times $t \geq 0$.

3. HAMMERSTEIN VIRTUAL ACTUATOR AND MAIN STABILITY RESULT

3.1 Reconfiguration Problem

An actuator *fault* or *failure* is modelled by means of changing the input map $\boldsymbol{B}$ towards $\boldsymbol{B}_f$ and changing the nonlinearity $\boldsymbol{f}$ towards $\boldsymbol{f}_f$. Columns of $\boldsymbol{B}_f$ that belong to faulty actuators are scaled in case of changes of the characteristic, or set to zero in case of actuator failure,

$$\dot{\boldsymbol{x}}_f(t) = \boldsymbol{A}\boldsymbol{x}_f(t) + \boldsymbol{B}_f \boldsymbol{f}_f\left(\boldsymbol{u}_f(t)\right) + \boldsymbol{B}_d \boldsymbol{d}(t), \quad \boldsymbol{x}_f(0) = \boldsymbol{x}_0 \tag{6a}$$

$$\boldsymbol{y}_f(t) = \boldsymbol{C}\boldsymbol{x}_f(t). \tag{6b}$$

The matrix $\boldsymbol{B}_f$ is usually rank-deficient. The input to the faulty plant is denoted as $\boldsymbol{u}_f(t)$. It differs from $\boldsymbol{u}_c(t)$, since, in general, the fault changes the loop behaviour. The nonlinear map $\boldsymbol{f}_f$, which reflects, for example, tighter actuation limits, is assumed to still satisfy Assumption 1.

After the fault, the closed loop formed by the faulty plant (6) and the nominal controller (5) is no longer adequate. In the case of actuator failures, the loop is partially open. The reconfiguration problem consists in finding a new controller that meets the original control goals as well as possible. In general, however, performance degradations are unavoidable.

The reconfiguration approach adopted here consists in augmenting the closed loop by means of a linear reconfiguration block with initial state $\boldsymbol{\zeta}_0$. This block is connected between the faulty plant (6) and the nominal controller (5) using the signal pairs $\boldsymbol{u}_f, \boldsymbol{y}_f$ and $\boldsymbol{u}_c, \boldsymbol{y}_c$. Together with the faulty plant, the reconfiguration block forms the *reconfigured plant*, to which the nominal controller (5) is connected via $\boldsymbol{u}_c, \boldsymbol{y}_c$ (Fig. 2).

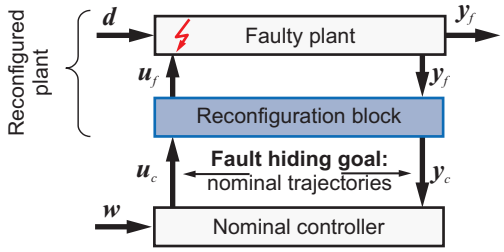

Fig. 2. Reconfigured control loop for fault-hiding.

Definition 2. (Fault-hiding goal). The reconfigured plant meets the fault-hiding goal, if it satisfies

$$\exists \boldsymbol{\zeta}_0 \text{ s.t. } \forall t, \ \boldsymbol{u}_c(t), \ \boldsymbol{x}_0 : \ \boldsymbol{y}(t) - \boldsymbol{y}_c(t) = \boldsymbol{0},$$

where $\boldsymbol{y}(t)$ is the nominal plant output under the same control input $\boldsymbol{u}_c(t)$ and same initial state $\boldsymbol{x}_0$.

If the fault-hiding goal is reached, the reconfigured plant behaviour equals the nominal plant behaviour from the controller perspective (Fig. 2). The reconfiguration problem is now stated as follows.

Problem 1. (Stabilising control reconfiguration). Given are the nominal Hammerstein plant (1), the nominal controller (5), and the faulty plant (6). Find a reconfiguration block that meets the fault-hiding goal and guarantees a globally asymptotically stable closed loop.

3.2 Hammerstein Virtual Actuator

This section extends the concept of the virtual actuator introduced in (Steffen, 2005) to Hammerstein plants (1). The virtual actuator is a realisation of the reconfiguration block in Fig. 3.

Definition 3. (Hammerstein virtual actuator). The *Hammerstein virtual actuator* is defined by the equations

$$\dot{\boldsymbol{x}}_\Delta(t) = \boldsymbol{A}\boldsymbol{x}_\Delta(t) + \boldsymbol{B}\boldsymbol{f}\left(\boldsymbol{u}_c(t)\right) - \boldsymbol{B}_f \boldsymbol{f}_f\left(\boldsymbol{M}\boldsymbol{x}_\Delta(t) + \boldsymbol{N}\boldsymbol{u}_c(t)\right) \tag{7a}$$

$$\boldsymbol{u}_f(t) = \boldsymbol{M}\boldsymbol{x}_\Delta(t) + \boldsymbol{N}\boldsymbol{u}_c(t) \tag{7b}$$

$$\boldsymbol{y}_c(t) = \boldsymbol{y}_f(t) + \boldsymbol{C}\boldsymbol{x}_\Delta(t) \tag{7c}$$

$$\boldsymbol{x}_\Delta(t) = \boldsymbol{x}(t) - \boldsymbol{x}_f(t), \quad \boldsymbol{x}_\Delta(0) = \boldsymbol{x}_{\Delta,0}. \tag{7d}$$

The virtual actuator synthesises lost control action by suitably distributing the control signal that is intended for faulty actuators to remaining actuators. It has two design freedoms: the feedback gain $\boldsymbol{M}$ and the feedforward gain $\boldsymbol{N}$. In the linear case (with $\boldsymbol{f}(\boldsymbol{u}) = \boldsymbol{u}$), a closed-loop separation principle follows, which implies that the reconfigured closed-loop poles consist of the nominal closed-loop poles, and poles of the virtual actuator that are unobservable from the controller. The gain $\boldsymbol{M}$ affects these additional poles, whereas the gain $\boldsymbol{N}$ affects the virtual actuator's zeros. The systematic use of these design freedoms for achieving various reconfiguration goals to shape the loop performance has been thoroughly studied for the linear case (Steffen, 2005; Lunze and Steffen, 2006; Lunze, 2006; Richter and Lunze, 2007; Richter et al., 2008).

To reflect the known input nonlinearities $\boldsymbol{f}, \boldsymbol{f}_f$ in the nominal and faulty plants (1), (6), the same maps $\boldsymbol{f}, \boldsymbol{f}_f$ are applied to the virtual actuator, whose difference state $\boldsymbol{x}_\Delta$ thus turns out to reflect the deviation of the faulty plant state $\boldsymbol{x}_f$ from the nominal plant state $\boldsymbol{x}$.

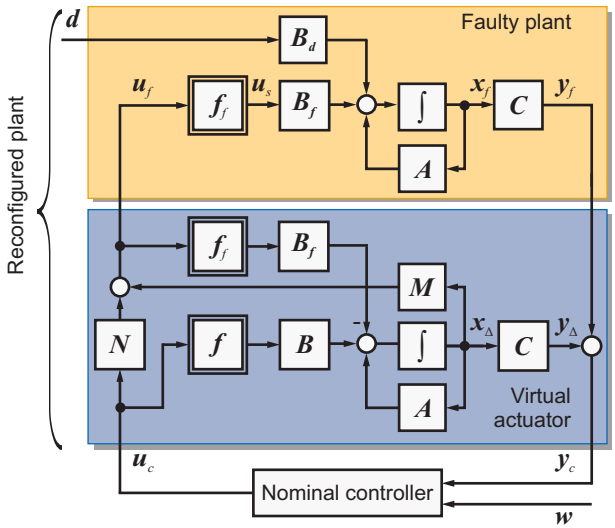

Fig. 3. Hammerstein virtual actuator as reconfiguration block.

With the Hammerstein virtual actuator as the reconfiguration block, Problem 1 is further specified as follows.

Problem 2. (Stabilising Hammerstein virtual actuator).
Given are the nominal Hammerstein plant (1), the nominal controller (5), and the faulty plant (6). Determine the parameters $\boldsymbol{M}$, $\boldsymbol{N}$, $\boldsymbol{x}_{\Delta,0}$ of the Hammerstein virtual actuator (7) such that the fault-hiding goal is met and the reconfigured closed loop (5), (6), (7) is globally asymptotically stable.

It will turn out below that the fault-hiding property is structurally satisfied for every choice of $\boldsymbol{M}$ and $\boldsymbol{N}$.

3.3 Main Result: Closed-Loop Stability

The main result consists in the following solution to Problem 2.

Theorem 1. (Reconfigured loop stability). Consider the reconfigured closed loop (5), (6), (7) shown in Fig. 3, where the diagonal matrix $0 \leq \boldsymbol{D} \in \mathbb{R}^{m\times m}$ must reflect the sector bounds of $\boldsymbol{f}_f$. Using Assumptions 1 and 2, the closed loop is globally asymptotically stable if $\boldsymbol{A}$ is Hurwitz, $(\boldsymbol{A}, \boldsymbol{B}_f)$ is controllable, and if there exist $\varepsilon > 0$, $\gamma_i \geq 0$, $\boldsymbol{\Gamma} = \operatorname{diag}(\gamma_i)$, $0 \prec \boldsymbol{P} \in \mathbb{R}^{n\times n}$, regular but otherwise arbitrary $\boldsymbol{L} \in \mathbb{R}^{(n\times l)}$, arbitrary $\boldsymbol{V} \in \mathbb{R}^{l\times n}$, such that the Kalman-Yakubovich-equations hold:

$$\boldsymbol{A}^T\boldsymbol{P} + \boldsymbol{P}\boldsymbol{A} = -\boldsymbol{L}\boldsymbol{L}^T - \varepsilon\boldsymbol{P} \tag{8a}$$

$$\boldsymbol{L}\boldsymbol{V} = (\boldsymbol{M} + \boldsymbol{\Gamma}\boldsymbol{M}\boldsymbol{A})^T - \boldsymbol{P}\boldsymbol{B}_f \tag{8b}$$

$$2\boldsymbol{D} + \boldsymbol{\Gamma}\boldsymbol{M}\boldsymbol{B}_f + \boldsymbol{B}_f^T\boldsymbol{M}^T\boldsymbol{\Gamma} = \boldsymbol{V}^T\boldsymbol{V}. \tag{8c}$$

The pair $(\boldsymbol{A}, \boldsymbol{M})$ must be observable. The reconfigured plant (6), (7) satisfies the fault-hiding goal if $\boldsymbol{x}_{\Delta,0} = \boldsymbol{0}$. ⋄

Before proving Theorem 1 in the following section, some remarks regarding its implications are made. Note that the virtual actuator design freedom $\boldsymbol{M}$ is part of the Equations (8a)–(8c). This fact is used in Section 5 to derive a design approach for $\boldsymbol{M}$ based on the Kalman-Yakubovich-equations.

Remark 1. The solution given for strict sector bounds is based on absolute stability. To add further robustness, hyperstability can be used, which requires the satisfaction of sector bounds in the mean as expressed in the Popov integral (Khalil, 2002). Then, Equations (8a)–(8c) must hold with $\boldsymbol{\Gamma} = \boldsymbol{0}$ and $\varepsilon = 0$.

Remark 2. The requirements of stability for $\boldsymbol{A}$, controllability for the pair $(\boldsymbol{A}, \boldsymbol{B}_f)$, and observability for the pair $(\boldsymbol{A}, \boldsymbol{M})$ are stricter than the stabilisability conditions of linear plants using linear virtual actuators. This conservatism arises from the fact that the stability-related result does not depend on every aspect of $\boldsymbol{f}_f$, but only on its sector bounds.

Remark 3. The requirement of complete controllability can be relaxed. Loss of controllability over distinct states is irrelevant if these states represent internal dynamics of failed actuators.

4. PROOF OF CLOSED-LOOP STABILITY AND THE FAULT-HIDING PROPERTY

4.1 Overview

Theorem 1 is proven by splitting stability of the reconfigured closed loop into several properties that are easier to prove. Section 4.2 provides a flow-based characterisation of the stability margin of linear systems to be used later. In Section 4.3, it is first shown that a separation principle holds for the closed loop, which implies that closed-loop stability is equivalent to nominal closed-loop stability (given by Assumption 2) and stability of a so-called difference system (to be shown). Section 4.4 describes how the difference system stability can be obtained in two steps. The first step consists in stabilising the unforced system (Section 4.5), whereas the second step takes into account exogenous inputs to the difference system (Section 4.6).

4.2 Stability Margin of Linear Systems

For any given point $\bar{\boldsymbol{x}}$ in the state-space, let E be the ellipsoid

$$E = \left\{ \boldsymbol{x} \,\middle|\, \sum_{i=1}^{n} \frac{x_i^2}{\alpha^2|\lambda_i|^2} = 1 \right\}, \text{ where } \alpha : \sum_{i=1}^{n} \frac{\bar{x}_i^2}{\alpha^2|\lambda_i|^2} = 1, \tag{9}$$

that passes through $\bar{\boldsymbol{x}}$ and whose main axes' lengths are given by the corresponding eigenvalues' magnitude $|\lambda_i|$ scaled by suitable factor α.

Lemma 2. (Flow of linear time-invariant systems). Consider a stable linear time-invariant system $(\boldsymbol{A}, \boldsymbol{B}, \boldsymbol{C})$ whose system matrix $\boldsymbol{A}$ has the real or pairwise conjugate complex eigenvalues $\lambda_1, \ldots, \lambda_n$. Then the inner product I of the flow $\boldsymbol{f}(\bar{\boldsymbol{x}}) = \boldsymbol{A}\bar{\boldsymbol{x}}$ at $\bar{\boldsymbol{x}}$ with the normal to the ellipsoid E in $\bar{\boldsymbol{x}}$ is bounded from below by the ratio

$$I \geq \left(\min_{i=1,\ldots,n} (|\lambda_i|) \right) / \left(\max_{j=1,\ldots,n} \left(|\lambda_{\text{real,j}}|, |\lambda_j|^2 / (|\operatorname{Re}(\lambda_j)|) \right) \right), \tag{10}$$

and the angular mismatch φ between the flow vector and the ellipsoid normal vector is bounded from above by the inequality

$$\cos(\varphi) \leq \left(\min_{i=1,\ldots,n} (|\lambda_i|) \right) / \left(\max_{j=1,\ldots,n} \left(|\lambda_{\text{real,j}}|, \frac{|\lambda_j|^2}{|\operatorname{Re}(\lambda_j)|} \right) \right), \tag{11}$$

where $\lambda_{\text{real,i}}$ is the ith real eigenvalue. ⋄

The bound depends on the ratio of the eigenvalue with smallest magnitude and the larger of either the eigenvalue with largest magnitude, or the eigenvalue pair with largest phase angle.

Proof. The proof uses the analytical expression for the normal to the tangent hyperplane T to E in $\bar{\boldsymbol{x}}$,

$$T = \left\{ \boldsymbol{x} \,\middle|\, \sum_{i=1}^{n} \frac{\bar{x}_i x_i}{\alpha^2|\lambda_i|^2} = 1 \right\}.$$

This description is brought into Hesse normal form by separation of the sum into an inner product

$$\begin{pmatrix} x_1 & x_2 & \ldots & x_n \end{pmatrix} \begin{pmatrix} \frac{\bar{x}_1}{|\lambda_1|^2} & \frac{\bar{x}_2}{|\lambda_2|^2} & \ldots & \frac{\bar{x}_n}{|\lambda_n|^2} \end{pmatrix}^T / \alpha^2 = 1.$$

The normal $\boldsymbol{n}$ to the ellipsoid E at point $\bar{\boldsymbol{x}}$ is described by

$$\boldsymbol{n} := \left(\frac{\bar{x}_1}{|\lambda_1|^2} \;\; \frac{\bar{x}_2}{|\lambda_2|^2} \;\; \cdots \;\; \frac{\bar{x}_n}{|\lambda_n|^2}\right)^T / \alpha^2. \tag{12}$$

The Hesse normal form is given with normalised vectors by

$$\boldsymbol{x}^T \boldsymbol{n}/\|\boldsymbol{n}\|_2 = 1/\|\boldsymbol{n}\|_2.$$

It is assumed that the matrix $\boldsymbol{A}$ has both real and conjugate complex eigenvalues. Without loss of generality, it is assumed that the kth and $(k+1)$th eigenvalues are a conjugate complex pair. Then it is always possible to transform $\boldsymbol{A}$ into the normal form

$$\boldsymbol{A} = \text{blockdiag}\left(\lambda_1 \;\; \cdots \;\; \begin{pmatrix} \text{Re}(\lambda_k) & \text{Im}(\lambda_k) \\ \text{Im}(\lambda_{k+1}) & \text{Re}(\lambda_{k+1}) \end{pmatrix} \;\; \cdots \;\; \lambda_n\right),$$

which results in the normalised flow at $\bar{\boldsymbol{x}}$

$$\boldsymbol{A}\bar{\boldsymbol{x}}/\|\boldsymbol{A}\bar{\boldsymbol{x}}\| = \begin{pmatrix} \bar{x}_1\lambda_1 \\ \cdots \\ \bar{x}_{k-1}\lambda_{k-1} \\ \bar{x}_k \,\text{Re}(\lambda_k) + \bar{x}_{k+1} \,\text{Im}(\lambda_k) \\ \bar{x}_k \,\text{Im}(\lambda_{k+1}) + \bar{x}_{k+1} \,\text{Re}(\lambda_{k+1}) \\ \bar{x}_{k+2}\lambda_{k+1} \\ \cdots \\ \bar{x}_n\lambda_n \end{pmatrix} / \|\boldsymbol{A}\bar{\boldsymbol{x}}\|.$$

Together with the normal (12) which points outwards, this flow leads to the inner product (denoted by $\langle\cdot,\cdot\rangle$) of normal and flow

$$I = -\langle \boldsymbol{n}, \boldsymbol{A}\bar{\boldsymbol{x}}\rangle/(\|\boldsymbol{n}\| \cdot \|\boldsymbol{A}\bar{\boldsymbol{x}}\|),$$

with

$$\begin{aligned}
\langle \boldsymbol{n}, \boldsymbol{A}\bar{\boldsymbol{x}}\rangle =& \frac{1}{\alpha^2}\left(\bar{x}_1^2/\lambda_1 + \ldots + \bar{x}_k^2 \frac{\text{Re}(\lambda_k)}{|\lambda_k|^2} + \bar{x}_k\bar{x}_{k+1}\frac{\text{Im}(\lambda_k)}{|\lambda_k|^2}\right. \\
&\left. + \bar{x}_k\bar{x}_{k+1}\frac{\text{Im}(\lambda_{k+1})}{|\lambda_{k+1}|^2} + \bar{x}_{k+1}^2\frac{\text{Re}(\lambda_{k+1})}{|\lambda_{k+1}|^2} + \ldots + \bar{x}_n^2/\lambda_n\right) \\
\|\boldsymbol{n}\| =& \frac{1}{\alpha^2}\sqrt{\bar{x}_1^2/|\lambda_1|^4 + \ldots + \bar{x}_n^2/|\lambda_n|^4} \\
\|\boldsymbol{A}\bar{\boldsymbol{x}}\| =& \left(\bar{x}_1^2\lambda_1^2 + \ldots + \bar{x}_k^2(\text{Re}(\lambda_k))^2 + 2\bar{x}_k\bar{x}_{k+1}\,\text{Re}(\lambda_k)\,\text{Im}(\lambda_k)\right. \\
&+ \bar{k}_{k+1}^2(\text{Im}(\lambda_k))^2 + \bar{x}_k^2(\text{Im}(\lambda_{k+1}))^2 + 2\bar{x}_k\bar{x}_{k+1}\,\text{Im}(\lambda_{k+1}) \\
&\left.\cdot\,\text{Re}(\lambda_{k+1}) + \bar{x}_{k+1}^2(\text{Re}(\lambda_{k+1}))^2 + \ldots + \bar{x}_n^2\lambda_n^2\right)^{\frac{1}{2}}.
\end{aligned}$$

Using the following facts about conjugate complex pairs, $|\lambda_k| = |\lambda_{k+1}|$, $\text{Re}(\lambda_k) = \text{Re}(\lambda_{k+1})$, $\text{Im}(\lambda_k) = -\,\text{Im}(\lambda_{k+1})$, and $(\text{Re}(\lambda_k))^2 + (\text{Im}(\lambda_k))^2 = |\lambda_k|^2$, the inner product simplifies to

$$\begin{aligned}
I =& -\frac{\left(\bar{x}_1^2/\lambda_1 + \ldots + (\bar{x}_k^2 + \bar{x}_{k+1}^2)\frac{\text{Re}(\lambda_k)}{|\lambda_k|^2} + \ldots + \bar{x}_n^2/\lambda_n\right)}{\sqrt{\bar{x}_1^2/|\lambda_1|^4 + \ldots + \bar{x}_n^2/|\lambda_n|^4}} \\
&/\sqrt{\bar{x}_1^2|\lambda_1|^2 + \ldots + \bar{x}_k^2|\lambda_k|^2 + \bar{x}_{k+1}^2|\lambda_{k+1}|^2 + \ldots + \bar{x}_n^2|\lambda_n|^2} \\
\geq& -\|\bar{\boldsymbol{x}}\|^2 \min_{i=1,\ldots,n}\left(\frac{1}{\lambda_{\min,\text{real}}}, \frac{\text{Re}(\lambda_i)}{|\lambda_i|^2}\right)\Big/\left(\|\bar{\boldsymbol{x}}\|^2\frac{\min_{i=1,\ldots,n}(|\lambda_i|)}{\min_{j=1,\ldots,n}\left(|\lambda_j|\right)^2}\right)
\end{aligned}$$

where $\lambda_{\min,\text{real}}$ is the smallest real eigenvalue. Reordering leads to the claimed bounds (10), (11). □

4.3 Closed-Loop Separation Principle

The following result shows that the virtual actuator with input saturation satisfies the fault-hiding principle and a separation principle.

Theorem 3. (Fault-hiding and separation principle). Stability of the reconfigured closed loop (5), (6), (7) is equivalent to stability of the nominal closed loop (1), (5) and stability of the difference system (15). The reconfigured plant (6), (7) meets the fault-hiding goal for all $\boldsymbol{M}$, $\boldsymbol{N}$ if $\boldsymbol{x}_{\Delta,0} = \boldsymbol{0}$. ⋄

Proof. The fault hiding property is seen by combination of the faulty plant (6) with the Hammerstein virtual actuator (7). Application of the linear transformation

$$\begin{pmatrix} \tilde{\boldsymbol{x}}(t) \\ \boldsymbol{x}_\Delta(t) \end{pmatrix} = \begin{pmatrix} \boldsymbol{I} & \boldsymbol{I} \\ \boldsymbol{0} & \boldsymbol{I} \end{pmatrix}\begin{pmatrix} \boldsymbol{x}_f(t) \\ \boldsymbol{x}_\Delta(t) \end{pmatrix} \tag{13}$$

results in the transformed reconfigured plant model

$$\begin{aligned}
\frac{d}{dt}\begin{pmatrix} \tilde{\boldsymbol{x}}(t) \\ \boldsymbol{x}_\Delta(t) \end{pmatrix} =& \begin{pmatrix} \boldsymbol{A} & \boldsymbol{0} \\ \boldsymbol{0} & \boldsymbol{A} \end{pmatrix}\begin{pmatrix} \tilde{\boldsymbol{x}}(t) \\ \boldsymbol{x}_\Delta(t) \end{pmatrix} - \begin{pmatrix} \boldsymbol{0} \\ \boldsymbol{B}_f \end{pmatrix}\boldsymbol{f}_f\left(\boldsymbol{M}\boldsymbol{x}_\Delta(t) + \boldsymbol{N}\boldsymbol{u}_c(t)\right) \\
&+ \begin{pmatrix} \boldsymbol{B} \\ \boldsymbol{B} \end{pmatrix}\boldsymbol{f}(\boldsymbol{u}_c(t)) + \begin{pmatrix} \boldsymbol{B}_d \\ \boldsymbol{0} \end{pmatrix}\boldsymbol{d}(t) \qquad (14a) \\
\begin{pmatrix} \boldsymbol{y}_f(t) \\ \boldsymbol{y}_c(t) \end{pmatrix} =& \begin{pmatrix} \boldsymbol{C} & -\boldsymbol{C} \\ \boldsymbol{C} & \boldsymbol{0} \end{pmatrix}\begin{pmatrix} \tilde{\boldsymbol{x}}(t) \\ \boldsymbol{x}_\Delta(t) \end{pmatrix}. \qquad (14b)
\end{aligned}$$

The first substate $\tilde{\boldsymbol{x}}$ has nominal input, system dynamics, output, and disturbance behaviour. Clearly for all $\boldsymbol{M}$, $\boldsymbol{N}$, it is independent of the difference system

$$\dot{\boldsymbol{x}}_\Delta(t) = \boldsymbol{A}\boldsymbol{x}_\Delta(t) - \boldsymbol{B}_f\boldsymbol{f}_f\left(\boldsymbol{M}\boldsymbol{x}_\Delta(t) + \boldsymbol{N}\boldsymbol{u}_c(t)\right) + \boldsymbol{B}\boldsymbol{f}\left(\boldsymbol{u}_c(t)\right) \tag{15}$$

whose dynamics are unobservable from the output $\boldsymbol{y}_c$ and not affected by the disturbance $\boldsymbol{d}(t)$. The nominal controller attached to the input $\boldsymbol{u}_c$ and the output $\boldsymbol{y}_c$ sees the system

$$\begin{aligned}
\dot{\tilde{\boldsymbol{x}}}(t) =& \boldsymbol{A}\tilde{\boldsymbol{x}}(t) + \boldsymbol{B}\boldsymbol{f}(\boldsymbol{u}_c(t)) + \boldsymbol{B}_d\boldsymbol{d}(t), \quad \tilde{\boldsymbol{x}}(0) = \boldsymbol{x}_0 + \boldsymbol{x}_{\Delta,0} \\
\boldsymbol{y}_c(t) =& \boldsymbol{C}\tilde{\boldsymbol{x}}(t),
\end{aligned}$$

which coincides with the nominal plant model (1) up to renaming the state if $\boldsymbol{x}_{\Delta,0} = \boldsymbol{0}$. It has hence been shown that fault-hiding is reached and the disturbance rejection is nominal. □

This separation, which only holds if the nonlinear maps $\boldsymbol{f}$, $\boldsymbol{f}_f$ in the virtual actuator equal the maps in the nominal and faulty plants, implies that the nominal controller may remain unchanged. Furthermore, the loop stabilisation task is split into two stabilisation tasks, namely

(1) to stabilise the disturbed nominal system $\tilde{\boldsymbol{x}}$ (solved by Assumption 2)
(2) to stabilise the difference system (15) (see next section).

4.4 Input-to-State Stability of the Difference System

It remains to deduce the stability of the difference system (15), which can be represented as the fictitious loop shown in Fig. 4.

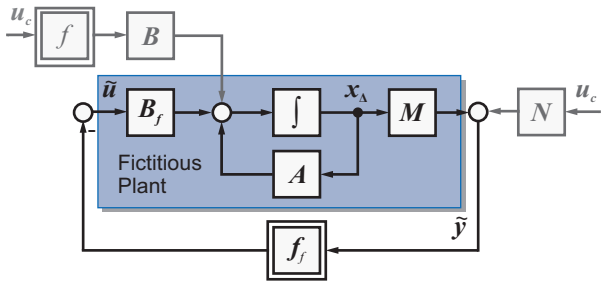

Fig. 4. Nonlinear difference system.

The fictitious loop (15) has a nonlinear characteristic $\boldsymbol{f}_f$ in the feedback branch as well as an exogenous disturbance input $\boldsymbol{u}_c$. In nonlinear systems, state stability in the sense of Lyapunov without inputs (henceforth referred to as *0-GAS* for global asymptotic stability without inputs) does not imply bounded-input-bounded-state stability. Hence, the paramount property of stability with respect to inputs must be ensured separately from the state stability in the sense of Lyapunov. To this end, the stability notions of *input-to-state-stability (ISS)* and

the *asymptotic gain* property (AG) are applied (Sontag, 1989, 1990).

The definition of ISS includes stability in the sense of Lyapunov. In other words, any ISS system is also 0-GAS, but not vice versa. To simplify the proof of ISS, an alternative characterisation due to Sontag and Wang (1996) is used.

Theorem 4. (Equivalent stability statements). For the forward-complete system (1) and a compact zero-invariant set $\mathcal{A} \subseteq \mathbb{R}^n$, the following properties are equivalent:

$$\{(ISS)\} \Leftrightarrow \{(0-GAS) \text{ and } (AG)\}.\diamond$$

Due to this result, it is possible to first consider 0-GAS in Section 4.5. The proof of Theorem 1 is completed in Section 4.6 with the validation of the AG property.

4.5 GAS of the Unforced System

Lemma 5. (0-GAS of the difference system). The control loop (15), where $\boldsymbol{A}$ is asymptotically stable, is *asymptotically stable* for $\boldsymbol{u}_c(t) \equiv \boldsymbol{0}$ and for $\frac{-\tilde{u}_i}{u_{f,i}} \leq \frac{1}{D_i}$, $i = 1, \ldots, m$ bounded by $\boldsymbol{D}$ in the first sector, if and only if the Kalman-Yakubovich-equations (8) are satisfied with ε, γ_i, $\boldsymbol{\Gamma}$, $\boldsymbol{P}$, $\boldsymbol{L}$, $\boldsymbol{V}$, $\boldsymbol{D}$, $(\boldsymbol{A}, \boldsymbol{B}_f)$, and $(\boldsymbol{A}, \boldsymbol{M})$ as stated in Theorem 1. $\diamond$

The proof follows immediately by identification of the problem at hand with standard problems of absolute stability (Khalil, 2002), where the stated stability conditions are obtained. The results are valid for stable linear multivariable forward branch-systems that have equal numbers of inputs and outputs. This is always true in the system (15) due to the dimensions of $\boldsymbol{M} \in \mathbb{R}^{m \times n}$ and $\boldsymbol{B}_f \in \mathbb{R}^{n \times m}$.

4.6 Asymptotic Gain Property

The stability properties of the forced difference system

$$\dot{\boldsymbol{x}}_\Delta(t) = \boldsymbol{A}\boldsymbol{x}_\Delta(t) - \underbrace{\boldsymbol{B}_f \boldsymbol{f}_f\left(\boldsymbol{M}\boldsymbol{x}_\Delta(t) + \boldsymbol{N}\boldsymbol{u}_c(t)\right) + \boldsymbol{B}\boldsymbol{f}\left(\boldsymbol{u}_c(t)\right)}_{\boldsymbol{l}(\boldsymbol{x}_\Delta, \boldsymbol{u}_c)} \quad (16)$$

are now investigated. This system consists of two superimposed dynamics: the autonomous part $\boldsymbol{A}\boldsymbol{x}_\Delta$, and the forced dynamics $\boldsymbol{l}(\boldsymbol{x}_\Delta, \boldsymbol{u}_c)$. The proof of stability separately uses an upper bound on the term $\boldsymbol{l}$.

Lemma 6. (AG of the disturbed difference system). The difference system (15) satisfies the AG property with respect to the input $\boldsymbol{u}_c$. The maximum deviation κ from the origin is given by

$$\kappa = |\boldsymbol{l}|_{\max} / \left(\|\boldsymbol{A}\|_2 \cdot |\cos(\varphi_{\max})|\right), \quad (17)$$

$$\cos(\varphi_{\max}) = \min_i \left(|\lambda_i|\right) / \left(\max_i \left(|\lambda_{\text{real},i}|, \frac{|\lambda_i|^2}{|\operatorname{Re}(\lambda_i)|}\right)\right)$$

$$|\boldsymbol{l}|_{\max} \leq \|\boldsymbol{A}\|_2 \cdot |\boldsymbol{x}_\Delta| \cdot |\cos(\varphi_{\max})|.\diamond$$

Proof. Since the vector field $\boldsymbol{A}\boldsymbol{x}_\Delta$ is linear and asymptotically stable, it is radially unbounded by any norm. This implies that $\dot{\boldsymbol{x}}_\Delta \leq \alpha(\|\boldsymbol{A}\boldsymbol{x}_\Delta\|)$ where $\alpha \in \mathcal{K}_\infty$, in other words, the state rate exceeds any bound as $|\boldsymbol{x}_\Delta| \to \infty$. For increasing $|\boldsymbol{x}_\Delta|$, the term $\boldsymbol{A}\boldsymbol{x}_\Delta$ finally dominates over the controlled radially bounded term $\boldsymbol{l}(\boldsymbol{x}_\Delta, \boldsymbol{u}_c)$.

In particular, $\forall \boldsymbol{\delta}\ \exists \kappa > 0 : |\boldsymbol{x}_\Delta| > \kappa \Rightarrow \dot{\boldsymbol{x}}_\Delta = \boldsymbol{A}\boldsymbol{x}_\Delta + \boldsymbol{\delta}$ where $|\boldsymbol{\delta}|$ may be chosen arbitrarily small. Hence, in the set $\bar{\mathcal{A}} := \{\boldsymbol{x}_\Delta : |\boldsymbol{x}_\Delta| > \kappa\}$ the system is governed by exponentially stable dynamics. This implies that the set $\mathcal{A} := \mathbb{R}^n - \bar{\mathcal{A}}$ is reached exponentially for any $\boldsymbol{x}_\Delta(0) \in \bar{\mathcal{A}}$, independently of $\boldsymbol{u}_c$.

The explicit upper bound (17) is obtained as follows. As established in Lemma 2, the eigenvalues of $\boldsymbol{A}$ determine the orientation of the flow vectors $\boldsymbol{A}\boldsymbol{x}_\Delta$ with respect to ellipsoids whose main axes are represented by the eigenvectors.

The angular deviation from the ellipsoid normal is bounded as given in Equation (11). The admissible flow disturbance (whose direction is unknown in general) is upper-bounded by the worst-case consideration, which results in a flow tangent to the corresponding contour line. Hence, the boundary to instability is described by the criterion

$$|\boldsymbol{l}|_{\max} \leq \|\boldsymbol{A}\|_2 \cdot |\boldsymbol{x}_\Delta| \cdot |\cos(\varphi_{\max})|, \quad (18)$$

which finally leads to the bound $|\boldsymbol{x}_\Delta| \geq \kappa$ with κ given in Equation (17). In summary, an asymptotic upper bound $\kappa \in \mathcal{K}_\infty$ on $\boldsymbol{x}_\Delta$ always exists, and the AG property holds. $\square$

5. SUMMARY OF HAMMERSTEIN VIRTUAL ACTUATOR DESIGN

The design procedure for the Hammerstein virtual actuator (7) is summarised in the following algorithm for the hyperstable case (see Remark 1).

Algorithm 1 Hammerstein virtual actuator design

Input: $\boldsymbol{A}$, $\boldsymbol{B}$, $\boldsymbol{C}$, $\boldsymbol{f}$, arbitrary regular $\boldsymbol{L}$

1: Initialise the nominal loop (1), (5), (7) with $\boldsymbol{B}_f = \boldsymbol{B}$, $\boldsymbol{f}_f = \boldsymbol{f}$, $\boldsymbol{M} = \boldsymbol{0}$, $\boldsymbol{N} = \boldsymbol{I}$, $\boldsymbol{x}(0) = \boldsymbol{x}_0$, $\boldsymbol{x}_\Delta(0) = \boldsymbol{0}$
2: **repeat**
3: Run the nominal control loop
4: **until** actuator fault f detected
5: Construct the actuator fault model $\boldsymbol{B}_f$, $\boldsymbol{f}_f$, its sector bounds $\boldsymbol{D}$, and update the virtual actuator (7)
6: Solve Equation (8c) for $\boldsymbol{V}$ with $\boldsymbol{\Gamma} = \boldsymbol{0}$
7: Solve Equation (8a) for $\boldsymbol{P}$ with $\varepsilon = 0$
8: Solve Equation (8b) for $\boldsymbol{M}$ with $\boldsymbol{\Gamma} = \boldsymbol{0}$
9: Update the virtual actuator (7) with $\boldsymbol{M}$ and arbitrary $\boldsymbol{N}$
10: Run the reconfigured control loop

Ensure: $(\boldsymbol{A}, \boldsymbol{M})$ observable; $(\boldsymbol{A}, \boldsymbol{B}_f)$ controllable

Result: GAS reconfigured closed loop (5), (6), (7)

6. EXPERIMENTAL EVALUATION

A successful application of Algorithm 1 to a laboratory system is presented in this section. The plant consists of tanks T_1, T_2 with levels h_1, h_2 interconnected by valves u_L, u_U, where T_1 is filled via pump u_P (Fig. 5). With state $\boldsymbol{x} = (h_1, h_2)^T$ and input vector $\boldsymbol{u} = (u_P, u_L, u_U)^T$, the plant is described around the operating point $\hat{\boldsymbol{x}} = (0.4, 0.06)^T$, $\hat{\boldsymbol{u}} = (0.48, 0.75, 0.2)^T$ by the linear model (1) with

$$\boldsymbol{A} = 10^3 \begin{pmatrix} -6.9 & 3.5 \\ 6.9 & -17.9 \end{pmatrix}, \quad \boldsymbol{B} = 10^3 \begin{pmatrix} 8.1 & -3.2 & -3.4 \\ 0 & 3.2 & 3.4 \end{pmatrix}, \quad \boldsymbol{B}_d = \begin{pmatrix} 1 \\ 0 \end{pmatrix}$$

$$\boldsymbol{B}_f = 10^3 \begin{pmatrix} 8.1 & 0 & 0 \\ 0 & 0 & 0 \end{pmatrix}, \quad \boldsymbol{C} = \begin{pmatrix} 1 & 0 \\ 0 & 1 \end{pmatrix}$$

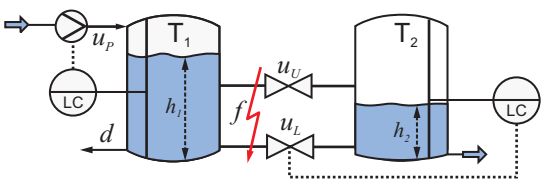

Fig. 5. Two-tank system with nominal control loops.

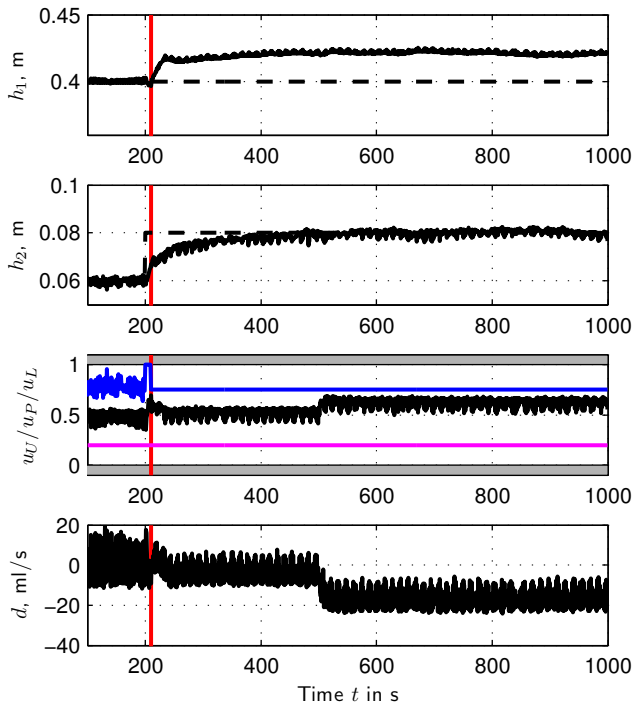

Fig. 6. Control reconfiguration to pump u_P after valves block.

and controlled by two linear decentralised controllers

$$\begin{pmatrix} u_P(t) \\ u_L(t) \\ u_U(t) \end{pmatrix} = \begin{pmatrix} 50 \cdot (w_1(t) - y_1(t)) + 4 \cdot \int_0^t (w_1(\tau) - y_1(\tau)) \mathrm{d}\tau \\ 0.5 \cdot (w_2(t) - y_2(t)) \\ 0 \end{pmatrix}.$$

The actuators are subject to saturations (3) with the lower and upper saturation limits relative to $\hat{\boldsymbol{u}}$

$$\underline{\boldsymbol{u}} = \begin{pmatrix} -0.48 & -0.75 & -0.2 \end{pmatrix}, \; \overline{\boldsymbol{u}} = \begin{pmatrix} 0.52 & 0.25 & 0.8 \end{pmatrix}.$$

The controlled quantities are the levels h_1, h_2, for which the control aims (i) stability, and (ii) regulation to a given setpoint, are formulated. In the experiment, the abrupt and non-transient fault is a failure of both valves ($f : u_L(t > t_f) = u_U(t > t_f) = 0$) at fault time $t_f = 210$ s. The plant is excited by a reference step of 0.02 m for the level h_2 at time $t = 200$ s. A leak of tank T_1 represents a disturbance d. Note that the fault breaks the loop and the reconfiguration method has to change the control loop structure to meet the control aims.

Fig. 6 shows the behaviour of the successfully reconfigured plant. Times $t < t_f$ correspond to steps 1-3 of Algorithm 1. When the valves block, the plant $(\boldsymbol{A}, \boldsymbol{B}_f)$ remains controllable. The application of steps 4-9 of Algorithm 1 with $\boldsymbol{L} = 2 \cdot \sqrt{|\lambda_{\min}|} \cdot \boldsymbol{I}_n$, where $\lambda_{\min}$ is the smallest eigenvalue of $\boldsymbol{A}$, and $\boldsymbol{D} = \boldsymbol{I}_m$, result in $\boldsymbol{M}$. The matrix $\boldsymbol{N}$, which may be arbitrary according to Algorithm 1, is designed according to (Steffen, 2005, Eq. (9.12)) to recover the equilibrium for h_2. The design results in

$$\boldsymbol{M} = \begin{pmatrix} 0.0609 & 0.4118 \\ 0.3975 & 0 \\ 0 & 0 \end{pmatrix}, \quad \boldsymbol{N} = \begin{pmatrix} 1 & 0.028 & 0.03 \\ 0 & 0 & 0 \\ 0 & 0 & 0 \end{pmatrix}. \tag{19}$$

The reference step causes the controller to open the lower valve up to the saturation limit until it blocks at t_f. After the fault and reconfiguration, the control action is redirected from the lower valve to the pump, as visible in Equation (19). The times $t > t_f$ in the plot correspond to step 10 in the algorithm. The remaining degree of freedom is assigned to the level h_2, which is tracked very well by the reconfigured closed loop. At $t_d = 500$ s, an outflow disturbance from the tank T_1 occurs (lower axis), which is very well rejected by pump speedup.

7. CONCLUSION

A new control reconfiguration method for stable Hammerstein systems after actuator faults has been shown. A design procedure was provided that guarantees the stability of the reconfigured control loop. The feasibility of the approach was experimentally shown. The systematic choice of the design freedom $\boldsymbol{L}$ in the Kalman-Yakubovich-equations, the use of the virtual actuator design freedom $\boldsymbol{N}$ to ensure that the loop equilibrium be recovered, and robustness aspects of the approach will be shown in a future publication. Current work explores further generalisations of the fault-hiding principle with respect to systems that are governed by nonlinear dynamics.

REFERENCES

A. Esna Ashari, A. Khaki Sedigh, and M. J. Yazdanpanah. Reconfigurable control system design using eigenstructure assignment: static, dynamic and robust approaches. *Int. J. Contr.*, 78(13):1005–1016, Sept. 2005. ISSN 0020-7179.

M. Blanke, M. Kinnaert, J. Lunze, and J. Staroswiecki. *Diagnosis and Fault-Tolerant Control*. Springer Verlag, Heidelberg, 2nd edition, 2006. ISBN 3-540-35652-5.

C. Bonivento, A. Isidori, L. Marconi, and A. Paoli. Implicit fault-tolerant control: application to induction motors. *Automatica*, 40(3):355–371, March 2004.

W. Chen and M. Saif. Adaptive actuator fault detection, isolation and accommodation in uncertain systems. *Int. J. Contr.*, 80(1):45–63, Jan. 2007.

B. Jiang, M. Staroswiecki, and V. Cocquempot. Fault accommodation for nonlinear dynamic systems. *IEEE Trans. Autom. Control*, 51(9):1578–1583, Sept. 2006.

H. K. Khalil. *Nonlinear Systems*. Prentice Hall, New Jersey, 3rd edition, 2002. ISBN 0130673897.

J. Lunze. Control reconfiguration after actuator failures: the generalised virtual actuator. In *Proc. 6th IFAC Symposium on Fault Detection, Supervision and Safety for Technical Processes*, pages 1309–1314, Beijing, 2006. IFAC.

J. Lunze and T. Steffen. Control reconfiguration after actuator failures using disturbance decoupling methods. *IEEE Trans. Autom. Control*, 51(10): 1590–1601, Oct. 2006.

H. E. Rauch. Autonomous control reconfiguration. *IEEE Control Systems Magazine*, 15(6):37–48, 1995.

J. H. Richter and J. Lunze. Markov-parameter-based control reconfiguration by matching the I/O-behaviour of the plant. In *Proc. Europ. Contr. Conf. (ECC) 2007*, pages 2942–2949, Kos, Greece, July 2-5 2007.

J. H. Richter, T. Schlage, and J. Lunze. Control reconfiguration of a thermofluid process by means of a virtual actuator. *IET Proceedings on Control Theory and Applications*, 1(6):1606–1620, November 2007.

J. H. Richter, J. Lunze, and T. Schlage. Control reconfiguration after actuator failures by Markov parameter matching. *International Journal of Control*, 2008. To appear.

M. Rodrigues, D. Theilliol, and D. Sauter. Fault tolerant control design for switched systems. In *Proc. 2nd IFAC Conf. on Analysis and Design of Hybrid Systems*, pages 223–228, Alghero, Italy, June 2006.

E. D. Sontag. Smooth stabilisation implies coprime factorization. *IEEE Trans. Autom. Control*, 34(4):435–443, Apr. 1989.

E. D. Sontag. Further facts about input to state stabilization. *IEEE Trans. Autom. Control*, 35(4):473–476, Apr. 1990.

E. D. Sontag and Y. Wang. New characterizations of input-to-state stability. *IEEE Trans. Autom. Control*, 41(9):1283–1294, Sept. 1996.

M. Staroswiecki, H. Yang, and B. Jiang. Progressive accommodation of aircraft actuator faults. In *Proc. 6th IFAC Symposium on Fault Detection Supervision and Safety for Technical Processes*, pages 877–882, Beijing, China, 2006.

T. Steffen. *Control Reconfiguration of Dynamical Systems: Linear Approaches and Structural Tests*, volume 320 of *Lecture Notes in Control and Information Sciences*. Springer-Verlag, Heidelberg, 2005. ISBN 3540257306.